

This item is the archived peer-reviewed author-version of:

Fusing spectral and textural information in near-infrared hyperspectral imaging to improve green tea classification modelling

Reference:

Mishra Puneet, Nordon Alison, Moh Asaari Mohd Shahrime, Lian Guoping, Redfern Sally.- Fusing spectral and textural information in near-infrared hyperspectral imaging to improve green tea classification modelling
Journal of food engineering - ISSN 0260-8774 - 249(2019), p. 40-47
Full text (Publisher's DOI): <https://doi.org/10.1016/J.JFOODENG.2019.01.009>
To cite this reference: <https://hdl.handle.net/10067/1585060151162165141>

Accepted Manuscript

Fusing spectral and textural information in near-infrared hyperspectral imaging to improve green tea classification modelling

Puneet Mishra, Alison Nordon, Mohd Shahrime Mohd Asaari, Guoping Lian, Sally Redfern



PII: S0260-8774(19)30015-9

DOI: <https://doi.org/10.1016/j.jfoodeng.2019.01.009>

Reference: JFOE 9507

To appear in: *Journal of Food Engineering*

Received Date: 25 October 2018

Revised Date: 6 January 2019

Accepted Date: 13 January 2019

Please cite this article as: Mishra, P., Nordon, A., Mohd Asaari, M.S., Lian, G., Redfern, S., Fusing spectral and textural information in near-infrared hyperspectral imaging to improve green tea classification modelling, *Journal of Food Engineering* (2019), doi: <https://doi.org/10.1016/j.jfoodeng.2019.01.009>.

This is a PDF file of an unedited manuscript that has been accepted for publication. As a service to our customers we are providing this early version of the manuscript. The manuscript will undergo copyediting, typesetting, and review of the resulting proof before it is published in its final form. Please note that during the production process errors may be discovered which could affect the content, and all legal disclaimers that apply to the journal pertain.

1 **Fusing spectral and textural information in near-infrared hyperspectral imaging to**
2 **improve green tea classification modelling**

3 Puneet Mishra^{1*}, Alison Nordon^{1*}, Mohd Shahrime Mohd Asaari², Guoping Lian^{3,4}, Sally
4 Redfern³

5 ¹*WestCHEM, Department of Pure and Applied Chemistry and Centre for Process Analytics*
6 *and Control Technology, University of Strathclyde, Glasgow, G1 1XL, United Kingdom*

7 ²*Vision Lab, Department of Physics, Campus Drie Eiken, University of Antwerp,*
8 *Edegemsesteenweg 200-240, 2610, Antwerp, Belgium*

9 ³*Unilever R&D Colworth, Colworth Science Park, Sharnbrook, Bedford, MK44 1LQ, United*
10 *Kingdom*

11 ⁴*Department of Chemical and Process Engineering, University of Surrey, Guildford GU2*
12 *7XH, United Kingdom*

13 *Corresponding authors email: puneet.mishra@strath.ac.uk , alison.nordon@strath.ac.uk*

14 **Abstract**

15 Hyperspectral imaging (HSI) can acquire data in two modes: imaging and spectroscopy,
16 revealing the spatially-resolved spectral properties of materials. Traditional HSI processing in
17 the close-range domain primarily focuses on the spectral information with minimal utilisation
18 of the spatial information present in the data. The present work describes a methodology for
19 utilising the spatial information present in HSI data to improve classification modelling over
20 that achievable with spectral information alone. The methodology has been evaluated using
21 near infrared (NIR) HSI data of sixteen green tea products from seven different countries.

22 The methodology involves selecting and sharpening an image plane to enhance the textural
23 details. The textural information is then extracted from the statistical properties of the grey
24 level co-occurrence matrix (GLCM) of the sharpened image plane using a moving window
25 operation. Finally, the textural properties are combined with the spectral information using
26 one of the three different levels of data fusion, i.e. raw data level, feature level and decision
27 level. Raw data-level fusion involved concatenating the spectral and textural data before
28 performing the classification task. The feature-level fusion involved performing principal
29 component analysis (PCA) on spectral and textural information and combining the PC scores
30 obtained prior to performing classification. Decision-level fusion involved a majority voting
31 scheme to enhance the final classification maps. All the classification tasks were performed
32 using multi-class support vector machine (SVM) models. The results showed that combining
33 the textural and spectral information during modelling resulted in improved classification of
34 the sixteen green tea products compared to models built using spectral or textural information
35 alone.

36 *Keywords:* chemical imaging; texture; support vector machine (SVM); grey level co-
37 occurrence matrix (GLCM); data fusion; green tea.

38 1. Introduction

39 Computer vision and image processing have benefited from the exploration of spatially-
40 resolved physical properties of materials in analytical chemistry [1]. The combination of
41 imaging with spectroscopy, known as hyperspectral imaging (HSI), has complemented
42 imaging by allowing simultaneous exploration of spatial and spectral properties of materials
43 in a fast and non-destructive way. Although HSI was primarily developed for remote sensing
44 [2], it is now a well-established technique in close-range laboratory settings [3, 4, 5, 6]. HSI

45 has been used for the study of a wide range of food products such as wheat flour [7], olive oil
46 [8], herbal tea [9], seeds [10], coffee [11], beans [12] and many more [13].

47 The information generated by HSI takes the form of hypercubes where the first two
48 dimensions represent the spatial information of the imaged scene and the third dimension
49 adds the spectral information to the pixels [12]. The extraction of meaningful information
50 from the hypercube requires advanced pattern recognition and data modelling. Although, HSI
51 data is rich in information, not all the information present is needed to perform the data
52 modelling. The traditional HSI processing approach includes selection of the region of
53 interest (ROI) over the image plane to extract the relevant spectra. The selected spectra are
54 then used to perform different types of modelling such as data visualisation, regression, and
55 classification. The models developed are used to predict the scores for each pixel to represent
56 prediction or classification maps [14]. This modelling approach aids in visualising the spatial
57 distribution of the predicted values or classes. However, the complementary information
58 present in the spatial domain, e.g., texture, is not generally used in the construction of
59 calibration models based on spectra [15]. In the predecessor of close-range HSI, i.e. remote
60 sensing, the importance of information present in the spatial domain of HSI is well realised.
61 In particular, utilising the spatial information to improve classification modelling is widely
62 employed [16]. The spatial information can be used either pre or post-classification
63 modelling to improve the classification accuracies and classification maps.

64 There are some extra benefits to the application of HSI in close-range settings, compared to
65 the remote-sensing domain, which further motivates the use of spatial information. One of the
66 benefits is the high spatial resolution of the images, which reduces the number of mixed
67 pixels in the imaged scene leading to improved image quality. The other is the artificial dark-
68 field illumination used to enhance the contrast of regions where illumination interferes with
69 the edges, scratches, imprints, slots and elevations over the imaging scene, leading to detailed

70 information about the physical features of samples [17]. The spatial information that is
71 primarily of interest in the case of close-range HSI is textural. Texture can be understood as a
72 quantitative measure of the arrangement of intensities in a region [18]. Therefore, it is
73 necessary to calculate texture from statistical analysis of an image plane. There are different
74 ways of extracting textural information from an image plane. Estimating the grey level co-
75 occurrence matrices (GLCMs) has gained widespread interest in the close-range HSI
76 processing domain [19, 20, 21, 22, 23, 24, 25]. A reason for its popularity is that the
77 statistical properties extracted from GLCMs can be used to represent, compare and classify
78 texture. Since the GLCM-based texture calculation can only be performed on a
79 monochromatic image, an image at a single wavelength is usually selected from the HS
80 image and subjected to GLCM analysis [20, 24]. Furthermore, utilising textural information
81 in conjunction with spectral information can be realised in a data fusion approach to combine
82 the two types of information at three different levels, i.e., low, middle and high. The low-
83 level data fusion of spectral and textural information utilises the spectral and textural data in
84 raw form and performs concatenation of the data matrices before the data modelling. Mid-
85 level fusion involves doing some feature transformation prior to performing the fusion such
86 as utilising principal component analysis (PCA) to capture the most important variation in the
87 feature vector and later concatenating the scores obtained for the corresponding features.
88 High-level involves decision-level fusion where the output from different models is usually
89 fused based on some decision criteria to enhance the final output such as classification maps.
90 The aim of this work is to present a methodology for fusing spectral and textural information
91 to improve the modelling of near-infrared (NIR) HSI data. To demonstrate the potential of
92 fusing textural and spectral information, the classification of sixteen green tea products from
93 seven different countries was considered. High-quality green tea products are mainly
94 characterised by the flavour that they impart, which involves two primary sensory

95 perceptions, i.e. taste and aroma. The distinct taste and aroma of any tea product are derived
96 from its geographical origin as they are unique to the climate and soil conditions in which the
97 plants were grown. Typically, discrimination of green tea products via sensory analysis is
98 performed using an expert human panel. Sensory analysis involves assessment of tea
99 products in leaf and/or extracted liquor form on the basis of appearance, colour, aroma and
100 taste, along with the overall quality of the samples. However, distinguishing tea products
101 based on sensory analysis is a time-consuming and expensive task as it requires an expert
102 human panel. Furthermore, sensory analysis is subjective, and it can be inconsistent and
103 unpredictable owing to physiological and psychological differences between tasters [26]. One
104 more limitation is that the expert panel cannot be used as an on-line technique for grading of
105 tea products [27]. In recent years, different analytical techniques have been explored for
106 assessment of tea products of which HSI is one. NIR HSI, in comparison to visible HSI,
107 provides access to the chemical information present in samples. NIR HSI has recently been
108 used to discriminate between different types of tea products [28], although only the spectral
109 information was used to build the classification models. However, leaf tea products also have
110 a rich amount of textural detail present in their leaves; such textural information has
111 previously been used to classify tea products [17, 29]. However, utilising texture alone is not
112 a robust modelling solution as textural properties are affected by variations in illumination
113 intensity [30]. Therefore, in this work, we utilise the textural information as supplementary
114 information to enhance NIR spectroscopy-based classification of green tea products.

115 2. Material and methods

116 2.1. Samples

117 Sixteen green tea samples, differing in geographical origin, were sourced in loose-leaf form
118 from Unilever R&D, Colworth Science Park, United Kingdom. All the samples were
119 provided in sealed packaging and were stored at ambient temperature until analysis. All

120 samples were green in colour and exhibited some textural differences owing to variations in
121 the shape and size of the leaves. The sixteen samples originated from seven different
122 countries: Argentina (one), South India (five), Sri Lanka (two), China (two), Japan (two),
123 Kenya (three) and Sumatra (one). Imaging experiments were performed by presenting the
124 sample in a circular black plastic cap (diameter = 3.3 cm, depth = 1.3 cm). The sixteen tea
125 samples were each analysed in a different cap to avoid any cross-contamination.

126 2.2. Hyperspectral imaging measurements

127 Imaging was performed with a push-broom line scan NIR HSI camera (*Model name: RED*
128 *EYE 1.7*) from INNO-SPEC (Nurnberg, Germany). The camera has an InGaAs sensor and
129 generates a spatial map of 320 x 256 pixels, and has pixel dimensions of 30 x 30 μm^2 . Images
130 were acquired over the spectral range of 950 – 1765 nm with a spectral resolution of 3.2 nm.
131 Two halogen light sources, each with a power of 50 W, were used to illuminate the samples.
132 For image acquisition, the sixteen tea samples were placed on the translation stage, which
133 was controlled via an independent stage motor system (Zolix TSA 200 BF). The speed of the
134 translation stage, 2.5 mm s⁻¹, was optimised using a checkerboard to avoid any distortion in
135 the shape of the image arising from the overlapping of spectral and spatial information. The
136 distance from the lens to the translation stage was 15 cm. Prior to acquisition of an image, a
137 set of white (Spectralon diffuse reflectance standard) and dark references were recorded for
138 radiometric calibration. Each image comprised more than 2000 pixels (spectra) per individual
139 green tea sample and was acquired using an integration time of 300 ms.

140 2.3. Data analysis

141 2.3.1. Image pre-processing

142 Variations in signal arising from illumination intensity, the detector sensitivity and the
143 transmission properties of the optics were corrected by radiometric calibration utilising dark
144 and white reference images. The correction was performed for every pixel in the HS image
145 according to equation (1):

$$146 \quad I_{R(i,j,k)} = \frac{I_{raw(i,j,k)} - I_{dark(i,j,k)}}{I_{white(i,j,k)} - I_{dark(i,j,k)}} \quad (1)$$

147 where, I_R is the calibrated reflectance, I_{raw} is the raw intensity measured from the test sample,
 148 I_{dark} is the intensity of the dark response, I_{white} is the intensity of the uniform white reference,
 149 and i and j are spatial coordinates and k is the wavelength of the image. The spectral range of
 150 the hypercube was reduced from 950 – 1765 nm to 967.11 – 1700 nm to remove noise. A
 151 moving window Savitzky-Golay (SAVGOL) filter [31] (15-point width and second order
 152 polynomial) was applied to each pixel of the image to remove random noise, e.g. spikes, from
 153 spectra. Further, to reduce light scattering effects arising from inhomogeneity of the sample
 154 surface, the spectra were normalised using the standard normal variate (SNV) [32].
 155 Smoothing and normalisation were performed using the *savgol* and *snv* functions,
 156 respectively, from PLS_Toolbox (version 8.11, Eigenvector Research Inc., USA).

157 2.3.2. Texture estimation

158 2.3.2.1. Selection of image plane

159 Textural analysis requires a single image plane to enable extraction of the GLCM properties.
 160 Since some spectral bands are noisy compared to others in HSI, the best image plane can be
 161 chosen on the basis of two different image quality parameters: the peak signal-to-noise ratio
 162 (PSNR) and the structural similarity index measure (SSIM). The PSNR and SSIM were
 163 calculated with respect to the mean image plane (reference image), obtained from averaging
 164 the intensities of pixels along the spectral dimension. The PSNR can be calculated using
 165 equation (2):

$$166 \quad PSNR = 10 \log_{10} \left(\frac{peakval^2}{MSE} \right) \quad (2)$$

167 where *peakval* is either specified by the user or selected from a range that is dependent on the
 170 image datatype (e.g. 255 for a uint8 image) and *MSE* is the mean square error between the
 171 chosen image plane and the reference image.

172 The SSIM [33] is based on the computation of three terms, namely the luminance term (l),
 173 the contrast term (c) and the structural term (s). The overall index is a multiplicative
 174 combination of the three terms calculated by equation (3):

$$175 \quad SSIM(x, y) = [l(x, y)]^\alpha \cdot [c(x, y)]^\beta \cdot [s(x, y)]^\gamma \quad (3)$$

176 where

$$177 \quad l(x, y) = \frac{2\mu_x\mu_y + C_1}{\mu_x^2 + \mu_y^2 + C_2}$$

178

$$179 \quad c(x, y) = \frac{2\sigma_x\sigma_y + C_2}{\sigma_x^2 + \sigma_y^2 + C_2}$$

180

$$181 \quad s(x, y) = \frac{\sigma_{xy} + C_3}{\sigma_x\sigma_y + C_3}$$

182

183 and μ_x and μ_y are the local means, and σ_x and σ_y are the standard deviations of images x
 184 (reference image) and y (chosen image plane), respectively, σ_{xy} is the cross-covariance for
 185 images x and y , α, β and γ are exponent terms, which were set to 1, and $C_1 = (k_1L)^2$, $C_2 =$
 186 $(k_2L)^2$ and $C_3 = C_2/2$ where $k_1 = 0.01$, $k_2 = 0.03$ and $L = 255$. The best image plane was
 187 selected based on the maximum PSNR and SSIM.

188

189 2.3.2.2. Sharpening of the image plane

190 The raw HS images obtained had soft edges owing to the limited focus and/or low spatial
 191 resolution of the camera resulting in low contrast between adjacent pixel intensities.
 192 Therefore, the image plane was sharpened to enhance the textural details. The enhanced
 193 textural details obtained with sharpening should result in more accurate calculation of the
 194 GLCM properties. Typically, the aim of sharpening is to increase the contrast along the edges
 195 where different colours meet. In the present work, the unsharp masking technique was used
 196 to perform image sharpening. This technique sharpens the image by first estimating a
 “blurred” negative image mask from the original image, which is then subtracted from the
 original image creating an image that is less blurry than the original [34]. Textural analysis

197 was then performed on the sharpened image via estimation of the statistical properties of the
198 GLCM.

199
200 2.3.2.3. Estimating GLCM properties
201

202 *Figure 1: Schematic of the window operation performed for extracting textural features.*

203 The textural information of the image has variations in the greyscale as a function of spatial
204 position. Different pixels in the image share spatial relationships in terms of greyscale
205 intensities, which is spatial correlation. A common method to represent the relationship
206 between greyscale pixels is via GLCMs [19, 20, 21, 22, 23, 24, 25]. The GLCM aims to
207 describe the textural information present in the image by defining how often pairs of pixels
208 with a specific value and spatial relationship occur in an image. The GLCM is a square
209 matrix whose elements represent the probabilities of a pixel being at a distance from another
210 pixel with a fixed spatial relationship. These values of the elements represent the conditional
211 probabilities of all pairwise combinations of greyscale levels in the spatial window. Statistical
212 measures can further be applied to these conditional probabilities to generate the textural
213 properties. In the present work, twenty different statistical measures were estimated resulting
214 in twenty different textural information maps. The twenty statistical properties considered
215 were the correlation, autocorrelation, contrast, cluster prominence, cluster shade,
216 dissimilarity, energy, entropy, homogeneity, variance, sum average, sum variance, sum
217 entropy, difference variance, difference entropy, two information measures of correlation,
218 inverse moment difference, inverse difference normalised and inverse difference moment
219 normalised. Further information on the use of statistical metrics for estimating textural
220 properties can be found in [35, 36, 37]. In the present work, the GLCM estimation was
221 performed utilising the “graycomatrix” command in Matlab (R2016b, Mathworks, USA). A
222 square window with a size of 11×11 pixels², which was moved over the image plane (see

223 Figure 1), was used for the GLCM estimation. The window size was selected based on the
224 number of pixels required to cover the largest tea leaves, and was an odd number to give
225 equal coverage of the pixels around the centre pixel. In this process, the greyscale intensity of
226 the centre pixel was replaced with the estimated textural property of the GLCM. To make the
227 GLCM uniform around the exterior area of the sample, a patch mask was defined, which
228 included replacing the individual pixel intensity values by their mean intensities. Textural
229 analysis resulted in the calculation of 20 image planes corresponding to the 20 statistical
230 metrics given above; all 20 textural image planes were used in subsequent analysis.

231 2.3.3. Feature transformation with PCA

232 In the present work, two PCA models were built to transform the spectral and textural
233 information separately. The number of principal components was selected such that >99% of
234 the variance in the data was retained. The PCA decomposition was performed in Matlab
235 utilising the PLS_Toolbox.

236 2.3.4. Data fusion scheme

237

238

239 *Figure 2: Schematic for raw data-level and feature-level fusion.*

240 Once the 20 textural features were obtained from the data, the fusion of textural information
241 with the spectral information was performed. The scheme for raw data-level and feature-level
242 fusion is depicted in Figure 2. Raw data-level fusion was performed by concatenating the
243 texture with the spectral information. In the case of feature-level fusion, two separate PCA
244 models were constructed to extract the relevant features from the spectral and textural cubes.
245 The extracted features were then concatenated before performing the classification
246 modelling. In the case of decision-level fusion, all the classification maps obtained from raw-
247 and feature-level data fusion were used within a majority voting scheme and the final

248 classification map was updated.

249 2.3.5. Classification with support vector machines

250 In the chemometrics domain, there are different methods to perform the classification of
251 spectral features [38]. However, in the image processing domain the support vector machine
252 (SVM) has gained popularity for the classification of fused spectral and textural information
253 [39]. Classification of the 16 green tea products was performed using multi-class error
254 correcting output code (ECOC) models containing SVM binary learners, using a one-versus-
255 one coding design. High dimensional mapping of the data was performed using a quadratic
256 kernel. For every green tea sample, spectra and/or textural information were extracted from
257 400 pixels, selected at random from the image, leading to 6400 pixels in total for the
258 calibration of the classification models. The models were cross-validated with the 10-fold
259 cross-validation method. This whole calibration procedure was performed with 100 iterations
260 with the mean validation accuracy and standard deviation recorded. The trained classifiers
261 were later used to generate the classification maps for the tea samples contained in the image,
262 which comprised more than 2000 pixels per sample. The ECOC-SVM models were
263 implemented in Matlab using the Statistics and Machine Learning Toolbox (R2016b).

264

265 3. Results

266

267

268 *Figure 3: Criteria used for selection of the best image plane on which to perform sharpening and textural analysis: a) SSIM*
269 *and b) PSNR for all image planes in the range 967.11 – 1700 nm.*

270 Figure 3 presents the SSIM and PSNR obtained for each HSI image plane in the range 967.11
271 – 1700 nm. It can be seen in Figure 3(a), that the SSIM value was highest for the image plane
272 at 1381 nm. The higher the SSIM value, the more similar the image of interest is to the

273 reference image. For example, an SSIM value of one signifies that the image is exactly the
274 same as the reference image, whereas, a SSIM value of zero indicates that there is no
275 similarity between the image plane and the reference image. In Figure 3(b), it can be seen
276 that the image plane at 1381 nm also has the highest PSNR value. A high PSNR value
277 indicates that there is more information present (relative to the noise) in the image plane at
278 1381 nm compared to image planes at other wavelengths. The image plane corresponding to
279 1381 nm is presented in Figure 4(a). Figure 4(b) presents the same image plane after
280 sharpening. It can be seen that before sharpening, the image plane is blurred, however, this is
281 reduced after sharpening and the textural details are more evident.

282
283

284 *Figure 4: Greyscale images produced using the image plane at 1381 nm (a) without and (b) with sharpening.*

285
286
287
288
289
290
291

Figure 5: Mean classification accuracies (in percent) of the 16 green tea products obtained for the calibration samples (pixels) using models built with raw data and PCA features. In both cases, models were built using spectral information alone, textural information alone and fused spectral and textural information. The error bars denote ± 1 standard deviation ($n = 100$).

292 Figure 5 presents the mean classification accuracies of the 16 green tea products obtained for
293 the calibration samples (pixels) using multi-class SVM models developed with spectral and
294 textural information. The accuracies are presented as the mean \pm one standard deviation for
295 100 iterations. Confusion matrices showing classification accuracies for individual classes
296 obtained using raw data and feature-level SVM models are given in Figures S1 and S2,
297 respectively, of the Supplementary Material. It can be seen from Figure 5 that the models
298 built with the spectral information alone were more accurate than those constructed using
299 only textural information. Combining textural information with spectral information resulted
300 in an improvement in the model accuracy. Improvements were observed for both raw data-
301 level fusion as well as feature-level fusion. The model accuracy for fusion of data at the raw

302 level was higher compared than that at the feature level. It could be that the features extracted
303 using PCA contain less information than the raw data. The features were selected so as to
304 retain 99% of the variance in the data whereas the raw data retains all of the information. and
305 therefore, this could account for the higher accuracy of the raw data models. Use of
306 supervised feature selection algorithms such as partial least squares discriminant analysis
307 (PLS-DA) could improve the performance of the feature-level models.

308
309 *Figure 6: Classification maps for the 16 green tea products obtained from SVM modelling of (a). raw spectral information,*
310 *(b). raw textural information, and (c). concatenated raw spectral and textural information.*

311
312
313 *Figure 7: Classification maps for the 16 green tea products obtained from SVM modelling of (a). PCA features extracted*
314 *from spectral information, (b). PCA features extracted from textural information, and (c). concatenated PCA features from*
315 *spectral and textural information.*

316
317
318 *Figure 8: Classification maps for the 16 green tea products obtained from decision-level data fusion, using a majority voting*
319 *scheme, of the six classification maps obtained from SVM modelling of spectral information, textural information, and*
320 *spectral and textural information using raw data (Figure 6) and PCA features (Figure 7).*

321
322 Figure 6 and Figure 7 presents the classification maps for the 16 green tea products obtained
323 from application of the raw data and feature-level SVM models, respectively, to the complete
324 image. Every circular object in the classification maps is a different green tea sample,
325 comprising more than 2000 pixels per sample, and the different colours reflect different
326 classes. In Figure 6, the three classification maps were obtained from three different SVM
327 models built using raw spectral data (Figure 6a), raw textural data (Figure 6b) and
328 concatenated raw spectral and textural data (Figure 6c). Similarly, in Figure 7 the three
329 classification maps were obtained from three different SVM models built using the scores
330 obtained from PCA of spectral data (Figure 7a), the scores obtained from PCA of textural
331 data (Figure 7b) and the concatenated scores obtained from separate PCA models of spectral
332 and textural data (Figure 7c). Figure 8 provides the output of a majority voting scheme
333 performed on all six classification maps, i.e., three from the raw data (Figure 6) and three

334 from the extracted features (Figure 7). Majority voting was performed by assigning the pixel
335 value to the class that occurred most frequently in all six classification maps. It can be seen
336 from visual inspection of Figures 6, 7 and 8 that improved classification maps (i.e. an
337 increase in the number of pixels inside the circular area belonging to the same class) were
338 obtained for models built using fused spectral and textural information. This improvement
339 can be quantified by calculating the percentage of correctly classified pixels as shown in
340 Figure 9. It can be seen that the highest values were obtained for models built using raw data-
341 level fusion (~84%), followed by decision-level fusion (~83%), with the least number of
342 correctly classified pixels obtained using feature-level data fusion (~78%). Fusion of spectral
343 and textural information at all levels (raw, feature and decision) gave improved model
344 accuracies compared to spectral or textural information alone at the relevant level (i.e. raw or
345 PCA features) leading to an improvement in the classification maps. These results are
346 consistent with HSI studies of meat products [20, 21, 23, 24, 25] where improved
347 classification or property prediction was obtained with models built using both spectral and
348 textural information.

349

350

351

352

353

354

Figure 9: Percentage of pixels correctly identified in the classification maps for the 16 green tea products obtained using six different SVM models and decision-level fusion by majority voting.

355 4. Conclusions

356 The spectral and spatial domains of HSI generate complementary information, and
357 synergistic processing of the information can lead to enhanced classification model
358 accuracies and improved classification maps. The present work fused spectral and textural
359 data at three different levels to demonstrate the usefulness of textural information in HSI for
360 classification of green teas. The highest classification accuracy ($97.30 \pm 0.12\%$ for the

361 calibration samples) was obtained using the raw data-level fusion, which was superior to that
362 obtained for feature-level data fusion. In this case, feature extraction resulted in information
363 loss. However, use of supervised feature selection methods, such as PLS-DA, could improve
364 the performance of the feature-level models. Decision-level fusion provided classification
365 maps of comparable quality to those obtained using raw data-level fusion. In conclusion, the
366 extracted textural information is always complementary as it can support the development of
367 enhanced understanding of the samples and further model improvement. However, it should
368 be noted that the decision to use the textural information in data modelling has to be based on
369 the samples imaged, as samples with high textural information can contribute positively to
370 model improvement whereas model with no such textural details will merely increase the
371 computation load. Therefore, the methodology developed will be useful in the assessment of
372 a variety of food products (e.g., tea, spices, meat and fruit) where consideration of both
373 spectral and textural information is required for, e.g., quality control and counterfeit
374 detection.

375 **Acknowledgment**

376 This work has received funding from the European Union's Horizon 2020 research and
377 innovation programme named 'MODLIFE' (Advancing Modelling for Process-Product
378 Innovation, Optimization, Monitoring and Control in Life Science Industries) under the Marie
379 Sklodowska-Curie grant agreement number 675251.

380 The authors also acknowledge the Centre for Hyperspectral Imaging at the University of
381 Strathclyde, particularly Julius Tschannerl and Prof. Stephen Marshall for their kind help in
382 performing the HSI experiments.

383 **References**

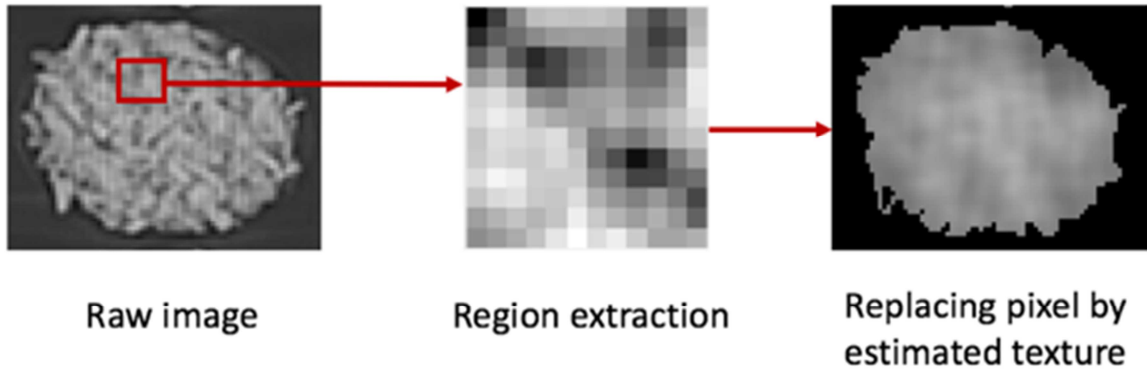
- 384 1. L.F. Capitán-Vallvey, N. López-Ruiz, A. Martínez-Olmos, M.M. Erenas, A.J. Palma,
385 Recent developments in computer vision-based analytical chemistry: A tutorial
386 review, *Anal. Chim. Acta.* 899 (2015) 23–56.
387 doi:<https://doi.org/10.1016/j.aca.2015.10.009>.
- 388 2. A.F. Goetz, G. Vane, J.E. Solomon, B.N. Rock, Imaging spectrometry for Earth
389 remote sensing., *Science.* 228 (1985) 1147–1153. doi:10.1126/science.228.4704.1147.
- 390 3. A.A. Gowen, C.P. O'Donnell, P.J. Cullen, G. Downey, J.M. Frias, Hyperspectral
391 imaging – an emerging process analytical tool for food quality and safety control,
392 *Trends Food Sci. Technol.* 18 (2007) 590–598.
393 doi:<https://doi.org/10.1016/j.tifs.2007.06.001>.
- 394 4. G. Elmasry, M. Kamruzzaman, D.-W. Sun, P. Allen, Principles and Applications of
395 Hyperspectral Imaging in Quality Evaluation of Agro-Food Products: A Review, *Crit.*
396 *Rev. Food Sci. Nutr.* 52 (2012) 999–1023. doi:10.1080/10408398.2010.543495.
- 397 5. Y.-Z. Feng, D.-W. Sun, Application of Hyperspectral Imaging in Food Safety
398 Inspection and Control: A Review, *Crit. Rev. Food Sci. Nutr.* 52 (2012) 1039–1058.
399 doi:10.1080/10408398.2011.651542.
- 400 6. M. Manley, Near-infrared spectroscopy and hyperspectral imaging: non-destructive
401 analysis of biological materials, *Chem. Soc. Rev.* 43 (2014) 8200–8214.
402 doi:10.1039/C4CS00062E.
- 403 7. P. Mishra, C.B.Y. Cordella, D.N. Rutledge, P. Barreiro, J.M. Roger, B. Diezma,
404 Application of independent components analysis with the JADE algorithm and NIR
405 hyperspectral imaging for revealing food adulteration, *J. Food Eng.* 168 (2016) 7–15.
- 406 8. D.M. Martínez Gila, P. Cano Marchal, J. Gámez García, J. Gómez Ortega, On-line
407 system based on hyperspectral information to estimate acidity, moisture and peroxides

- 408 in olive oil samples, *Comput. Electron. Agric.* 116 (2015) 1–7.
409 doi:<https://doi.org/10.1016/j.compag.2015.06.002>.
- 410 9. M. Sandasi, W. Chen, I. Vermaak, A. Viljoen, Non-destructive quality assessment of
411 herbal tea blends using hyperspectral imaging, *Phytochem. Lett.* 24 (2018) 94–101.
412 doi:<https://doi.org/10.1016/j.phytol.2018.01.016>.
- 413 10. C. Nansen, G. Zhao, N. Dakin, C. Zhao, S.R. Turner, Using hyperspectral imaging to
414 determine germination of native Australian plant seeds, *J. Photochem. Photobiol. B*
415 *Biol.* 145 (2015) 19–24. doi:<https://doi.org/10.1016/j.jphotobiol.2015.02.015>.
- 416 11. N. Caporaso, M.B. Whitworth, M.S. Fowler, I.D. Fisk, Hyperspectral imaging for
417 non-destructive prediction of fermentation index, polyphenol content and antioxidant
418 activity in single cocoa beans, *Food Chem.* 258 (2018) 343–351.
419 doi:<https://doi.org/10.1016/j.foodchem.2018.03.039>.
- 420 12. K. Phuangsombut, T. Ma, T. Inagaki, S. Tsuchikawa, A. Terdwongworakul, Near-
421 infrared hyperspectral imaging for classification of mung bean seeds, *Int. J. Food*
422 *Prop.* 21 (2018) 799–807. doi:[10.1080/10942912.2018.1476378](https://doi.org/10.1080/10942912.2018.1476378).
- 423 13. Y. Liu, H. Pu, D.-W. Sun, Hyperspectral imaging technique for evaluating food
424 quality and safety during various processes: A review of recent applications, *Trends*
425 *Food Sci. Technol.* 69 (2017) 25–35. doi:<https://doi.org/10.1016/j.tifs.2017.08.013>.
- 426 14. J.M. Amigo, H. Babamoradi, S. Elcoroaristizabal, Hyperspectral image analysis. A
427 tutorial, *Anal. Chim. Acta.* 896 (2015) 34–51.
428 doi:<https://doi.org/10.1016/j.aca.2015.09.030>.
- 429 15. A. de Juan, Hyperspectral image analysis. When space meets Chemistry, *J. Chemom.*
430 32 (2018) e2985–n/a. doi:[10.1002/cem.2985](https://doi.org/10.1002/cem.2985).

- 431 16. L. Wang, C. Shi, C. Diao, W. Ji, D. Yin, A survey of methods incorporating spatial
432 information in image classification and spectral unmixing, *Int. J. Remote Sens.* 37
433 (2016) 3870–3910. doi:10.1080/01431161.2016.1204032.
- 434 17. A. Laddi, S. Sharma, A. Kumar, P. Kapur, Classification of tea grains based upon
435 image texture feature analysis under different illumination conditions, *J. Food Eng.*
436 115 (2013) 226–231. doi:https://doi.org/10.1016/j.jfoodeng.2012.10.018.
- 437 18. M. Tuceryan, A.K. Jain, Texture analysis, in: *Handb. Pattern Recognit. Comput. Vis.*,
438 World Scientific, 1993: pp. 235–276.
- 439 19. J. Ma, D.-W. Sun, J.-H. Qu, H. Pu, Prediction of textural changes in grass carp fillets
440 as affected by vacuum freeze drying using hyperspectral imaging based on integrated
441 group wavelengths, *LWT - Food Sci. Technol.* 82 (2017) 377–385.
442 doi:https://doi.org/10.1016/j.lwt.2017.04.040.
- 443 20. C. Garrido-Novell, A. Garrido-Varo, D. Pérez-Marín, J.E. Guerrero, Using spectral
444 and textural data extracted from hyperspectral near infrared spectroscopy imaging to
445 discriminate between processed pork, poultry and fish proteins, *Chemom. Intell. Lab.*
446 *Syst.* 172 (2018) 90–99. doi:https://doi.org/10.1016/j.chemolab.2017.11.011.
- 447 21. D. Yang, D. He, A. Lu, D. Ren, J. Wang, Combination of spectral and textural
448 information of hyperspectral imaging for the prediction of the moisture content and
449 storage time of cooked beef, *Infrared Phys. Technol.* 83 (2017) 206–216.
450 doi:https://doi.org/10.1016/j.infrared.2017.05.005.
- 451 22. S. Fan, B. Zhang, J. Li, C. Liu, W. Huang, X. Tian, Prediction of soluble solids
452 content of apple using the combination of spectra and textural features of
453 hyperspectral reflectance imaging data, *Postharvest Biol. Technol.* 121 (2016) 51–61.
454 doi:https://doi.org/10.1016/j.postharvbio.2016.07.007.

- 455 23. D. Liu, H. Pu, D.-W. Sun, L. Wang, X.-A. Zeng, Combination of spectra and texture
456 data of hyperspectral imaging for prediction of pH in salted meat, *Food Chem.* 160
457 (2014) 330–337. doi:<https://doi.org/10.1016/j.foodchem.2014.03.096>.
- 458 24. H. Pu, D.-W. Sun, J. Ma, J.-H. Cheng, Classification of fresh and frozen-thawed pork
459 muscles using visible and near infrared hyperspectral imaging and textural analysis,
460 *Meat Sci.* 99 (2015) 81–88. doi:<https://doi.org/10.1016/j.meatsci.2014.09.001>.
- 461 25. W. Cheng, D.-W. Sun, H. Pu, Y. Liu, Integration of spectral and textural data for
462 enhancing hyperspectral prediction of K value in pork meat, *LWT - Food Sci.*
463 *Technol.* 72 (2016) 322–329. doi:<https://doi.org/10.1016/j.lwt.2016.05.003>.
- 464 26. D. Huo, Y. Wu, M. Yang, H. Fa, X. Luo, C. Hou, Discrimination of Chinese green tea
465 according to varieties and grade levels using artificial nose and tongue based on
466 colorimetric sensor arrays, *Food Chem.* 145 (2014) 639–645.
467 doi:<https://doi.org/10.1016/j.foodchem.2013.07.142>.
- 468 27. W. He, X. Hu, L. Zhao, X. Liao, Y. Zhang, M. Zhang, J. Wu, Evaluation of Chinese
469 tea by the electronic tongue: Correlation with sensory properties and classification
470 according to geographical origin and grade level, *Food Res. Int.* 42 (2009) 1462–
471 1467. doi:<https://doi.org/10.1016/j.foodres.2009.08.008>.
- 472 28. P. Mishra, A. Nordon, J. Tschannerl, G. Lian, S. Redfern, S. Marshall, Near-infrared
473 hyperspectral imaging for non-destructive classification of commercial tea products,
474 *J. Food Eng.* 238 (2018) 70–77. doi:<https://doi.org/10.1016/j.jfoodeng.2018.06.015>.
- 475 29. Z. Tang, Y. Su, M.J. Er, F. Qi, L. Zhang, J. Zhou, A local binary pattern based texture
476 descriptors for classification of tea leaves, *Neurocomputing.* 168 (2015) 1011–1023.
477 doi:<https://doi.org/10.1016/j.neucom.2015.05.024>.
- 478 30. N.R. Sarkar, Machine vision for quality control in the food industry, *Instrum.*
479 *Methods Qual. Assur. Foods.* (1991) 167–187.

- 480 31. A. Savitzky, M.J.E. Golay, Smoothing and Differentiation of Data by Simplified
481 Least Squares Procedures., *Anal. Chem.* 36 (1964) 1627–1639.
482 doi:10.1021/ac60214a047.
- 483 32. R.J. Barnes, M.S. Dhanoa, S.J. Lister, Standard Normal Variate Transformation and
484 De-Trending of Near-Infrared Diffuse Reflectance Spectra, *Appl. Spectrosc.* 43
485 (1989) 772–777. doi:10.1366/0003702894202201.
- 486 33. Z. Wang, A.C. Bovik, H.R. Sheikh, E.P. Simoncelli, Image quality assessment: from
487 error visibility to structural similarity, *IEEE Trans. Image Process.* 13 (2004) 600–
488 612. doi:10.1109/TIP.2003.819861.
- 489 34. A. Polesel, G. Ramponi, V.J. Mathews, Image enhancement via adaptive unsharp
490 masking, *IEEE Trans. Image Process.* 9 (2000) 505–510. doi:10.1109/83.826787.
- 491 35. D.A. Clausi, An analysis of co-occurrence texture statistics as a function of grey level
492 quantization, *Can. J. Remote Sens.* 28 (2002) 45–62. doi:10.5589/m02-004.
- 493 36. L.K. Soh, C. Tsatsoulis, Texture analysis of SAR sea ice imagery using gray level co-
494 occurrence matrices, *IEEE Trans. Geosci. Remote Sens.* 37 (1999) 780–795.
495 doi:10.1109/36.752194.
- 496 37. R.M. Haralick, K. Shanmugam, I. Dinstein, Textural Features for Image
497 Classification, *IEEE Trans. Syst. Man. Cybern.* SMC-3 (1973) 610–621.
498 doi:10.1109/TSMC.1973.4309314.
- 499 38. F. Marini, Classification methods in chemometrics, *Curr. Anal. Chem.* 6 (2010) 72–
500 79.
- 501 39. R. Seifi Majdar, H. Ghassemian, A probabilistic SVM approach for hyperspectral
502 image classification using spectral and texture features, *Int. J. Remote Sens.* 38 (2017)
503 4265–4284. doi:10.1080/01431161.2017.1317941.



505

506 Figure 1 : Schematic of the window operation performed for extracting textural features.

507

508

509

510

511

512

513

514

515

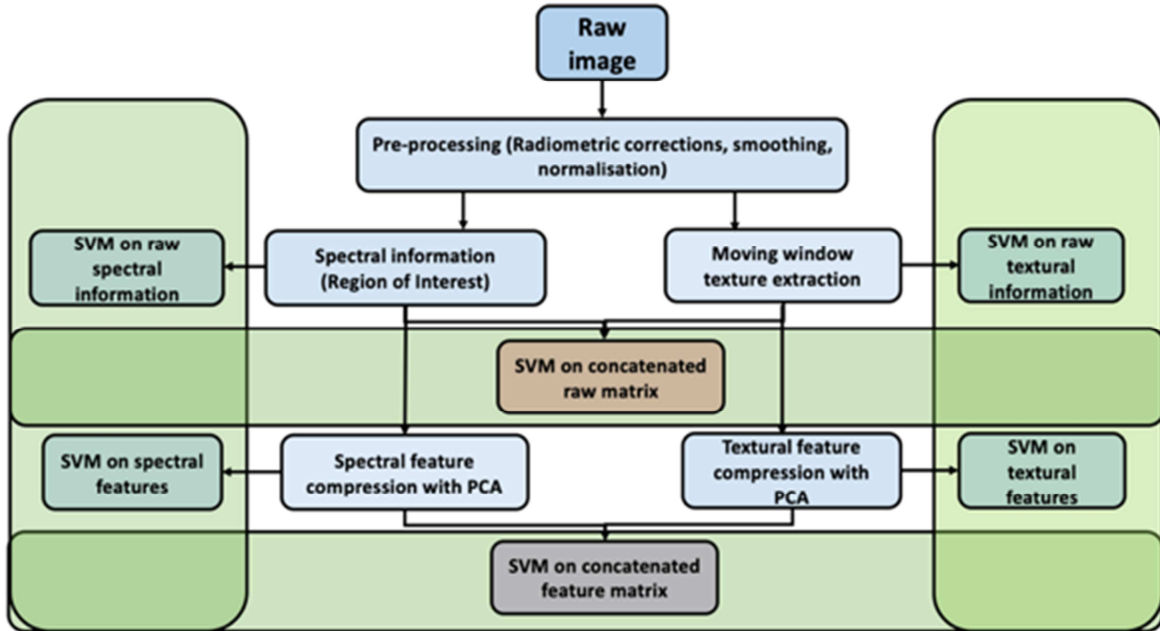
516

517

518

519

520



521

522 Figure 2: Schematic for raw data-level and feature-level fusion.

523

524

525

526

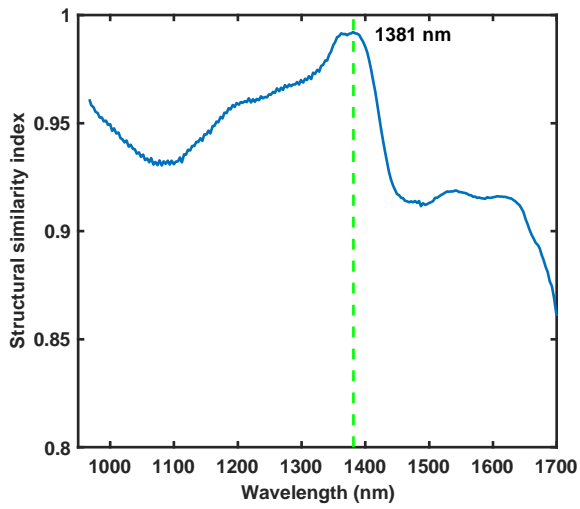
527

528

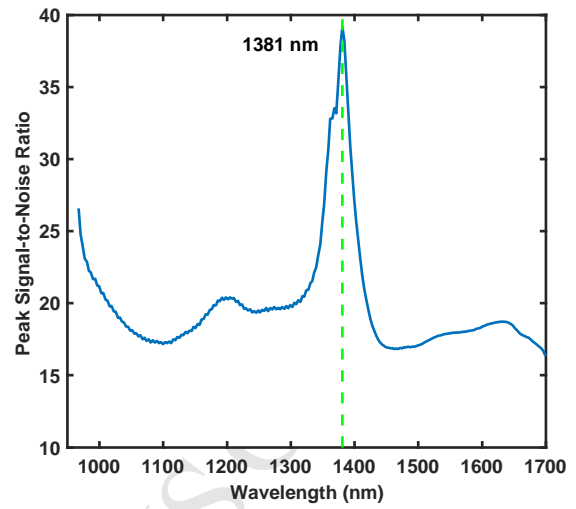
529

530

531



532



533

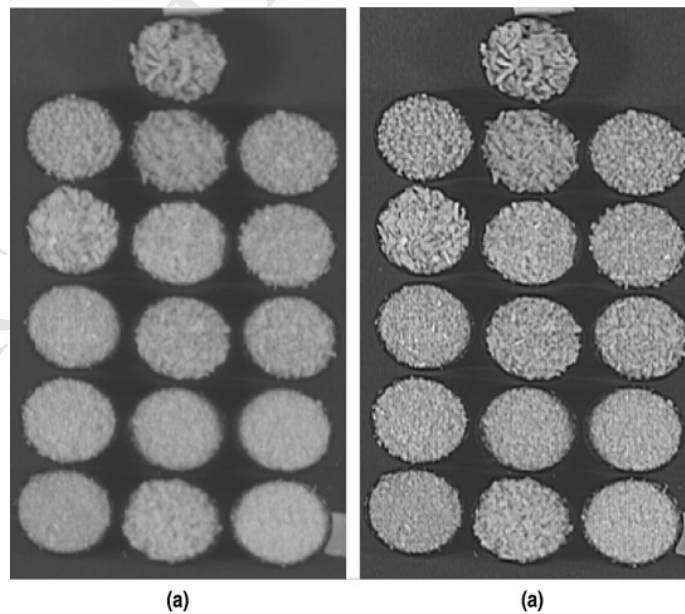
(a)

(b)

534 Figure 3 : Criteria used for selection of the best image plane on which to perform sharpening
 535 and textural analysis: a) SSIM and b) PSNR for all image planes in the range 967.11 – 1700
 536 nm.

537

538

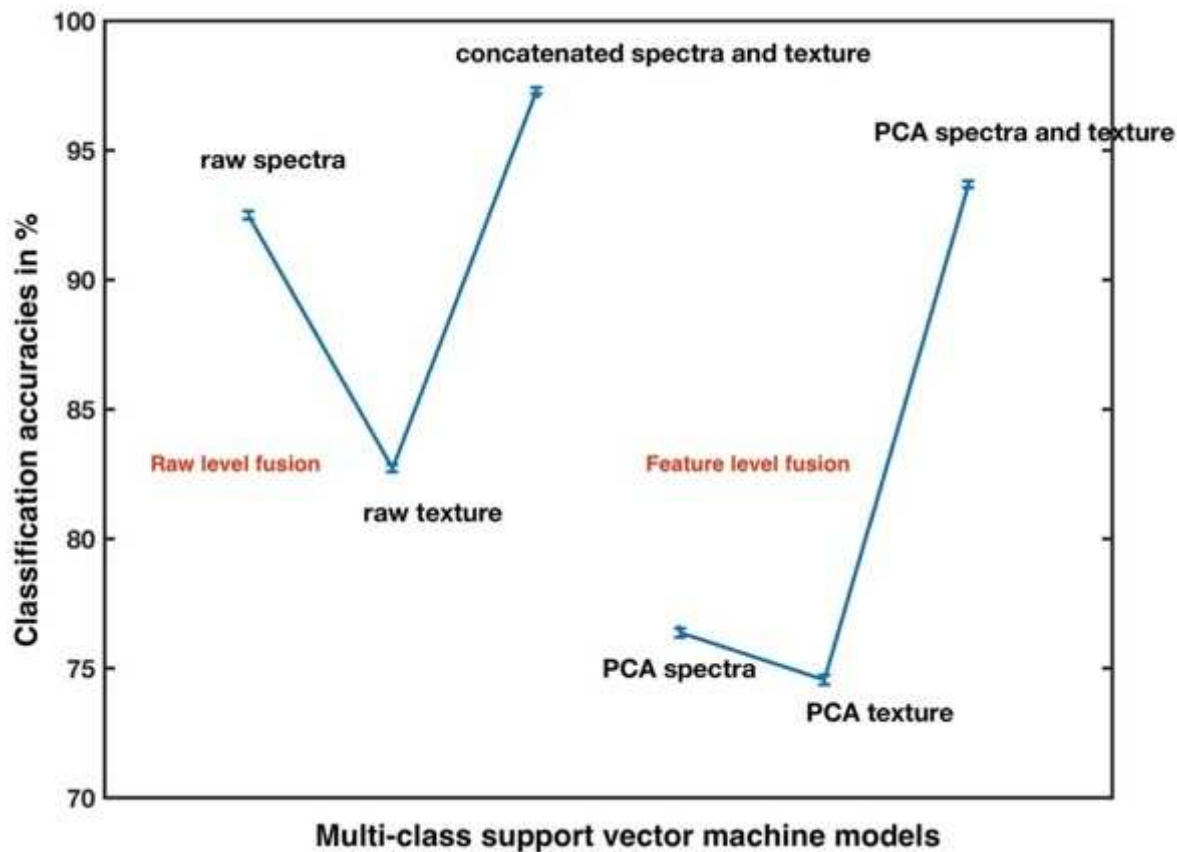


539

540 Figure 4 : Greyscale images produced using the image plane at 1381 nm (a) without and (b)

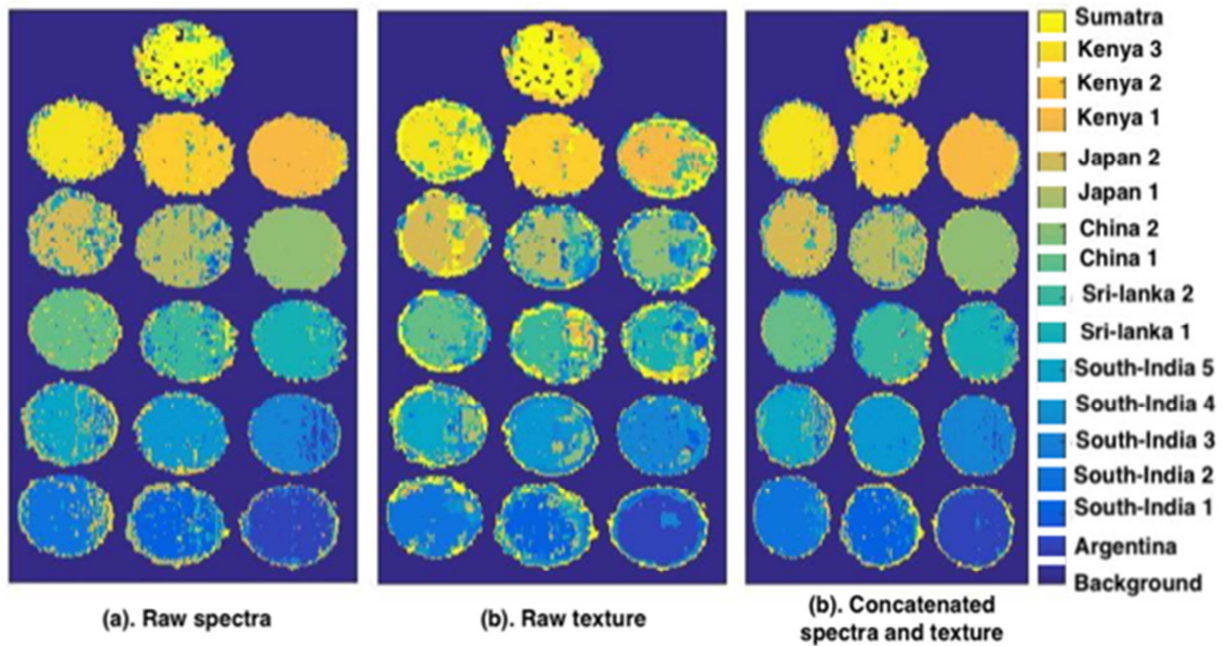
541 with sharpening.

542



543
544 Figure 5 : Mean classification accuracies (in percent) of the 16 green tea products obtained
545 for the calibration samples (pixels) using models built with raw data and PCA features. In
546 both cases, models were built using spectral information alone, textural information alone
547 and fused spectral and textural information. The error bars denote ± 1 standard deviation ($n =$
548 100).
549

550

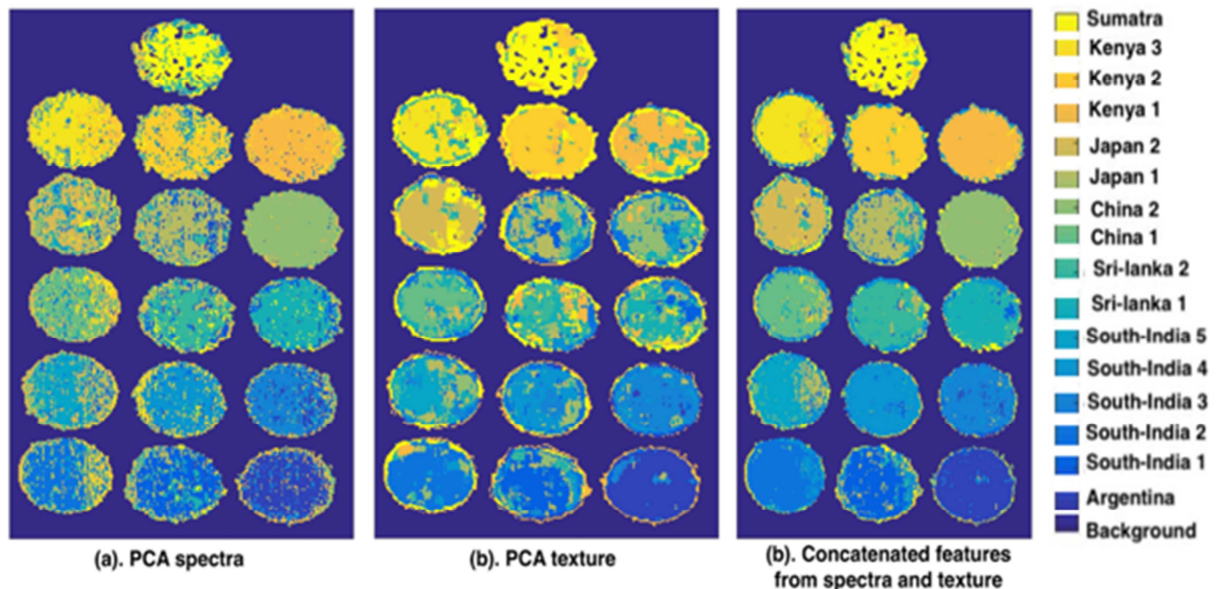


551
552

553 Figure 6 : Classification maps for the 16 green tea products obtained from SVM modelling of
554 (a). raw spectral information, (b). raw textural information, and (c). concatenated raw spectral
555 and textural information.

556

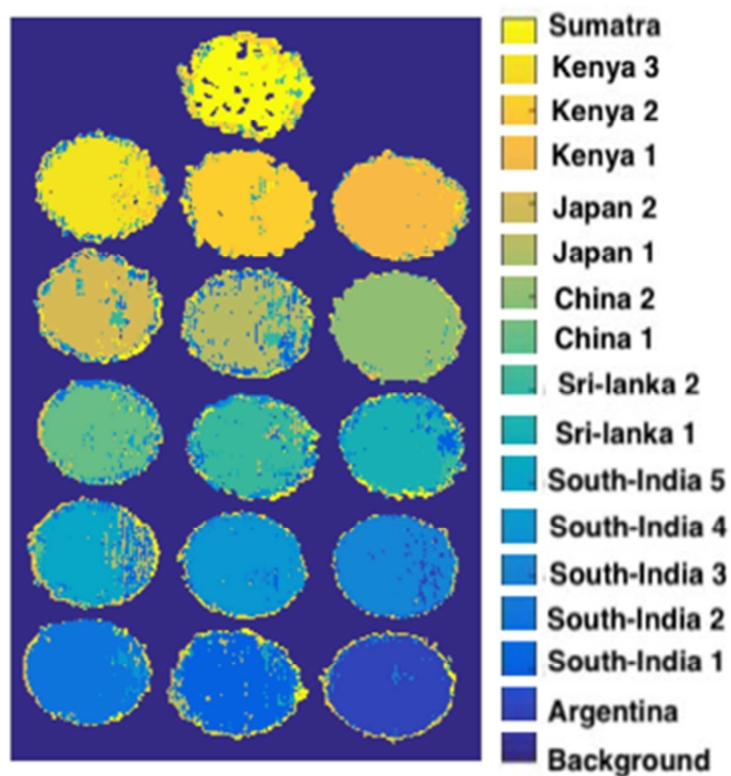
557



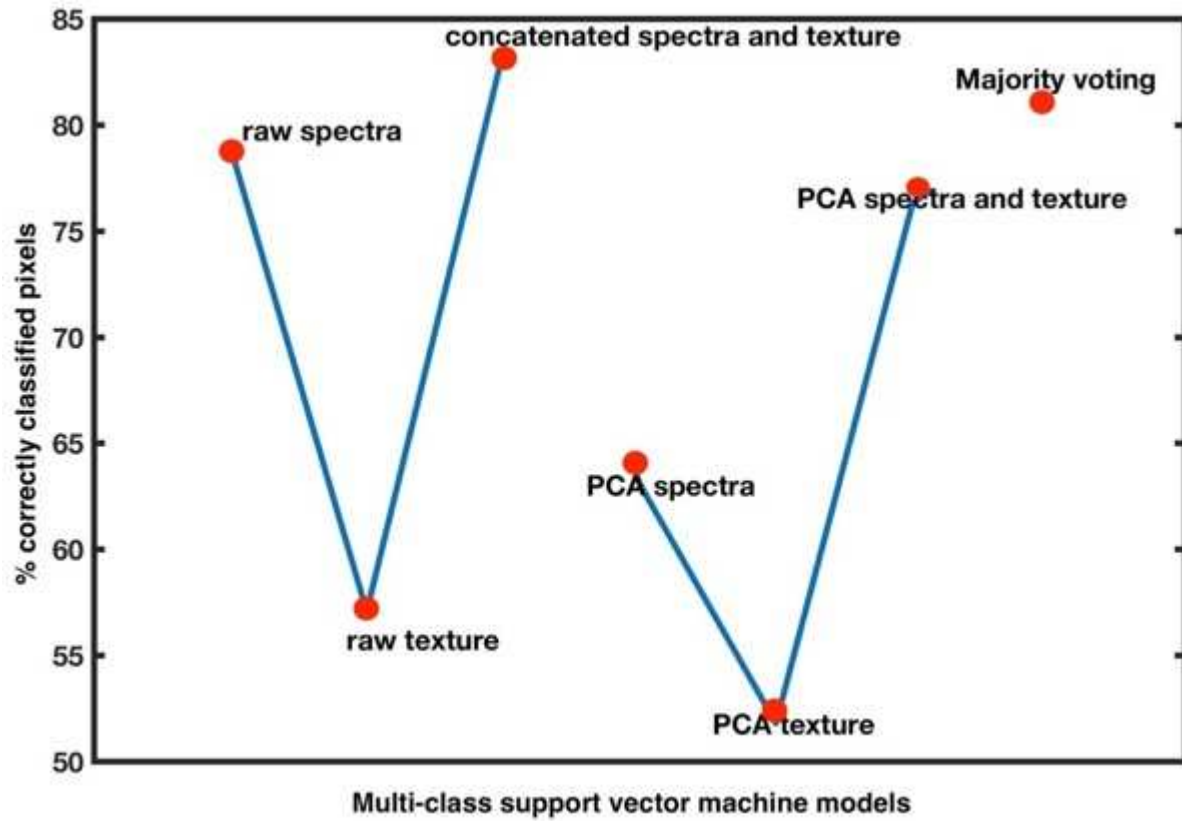
558
559

560 Figure 7 : Classification maps for the 16 green tea products obtained from SVM modelling of
561 (a). PCA features extracted from spectral information, (b). PCA features extracted from
562 textural information, and (c). concatenated PCA features from spectral and textural
563 information.

564

565
566

567 Figure 8 : Classification maps for the 16 green tea products obtained from decision-level data
568 fusion, using a majority voting scheme, of the six classification maps obtained from SVM
569 modelling of spectral information, textural information, and spectral and textural information
570 using raw data (Figure 6) and PCA features (Figure 7).



571
572
573
574
575
576

Figure 9 : Percentage of pixels correctly identified in the classification maps for the 16 green tea products obtained using six different SVM models and decision-level fusion by majority voting.

577

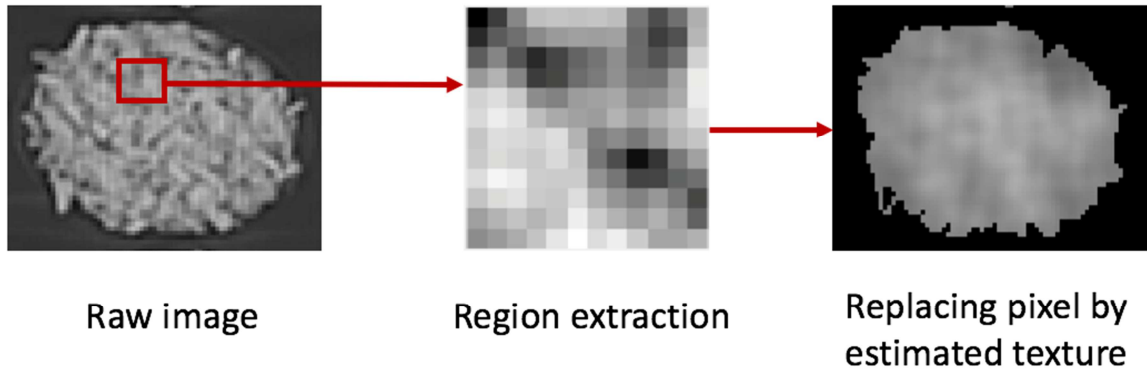


Figure 1 : Schematic of the window operation performed for extracting textural features.

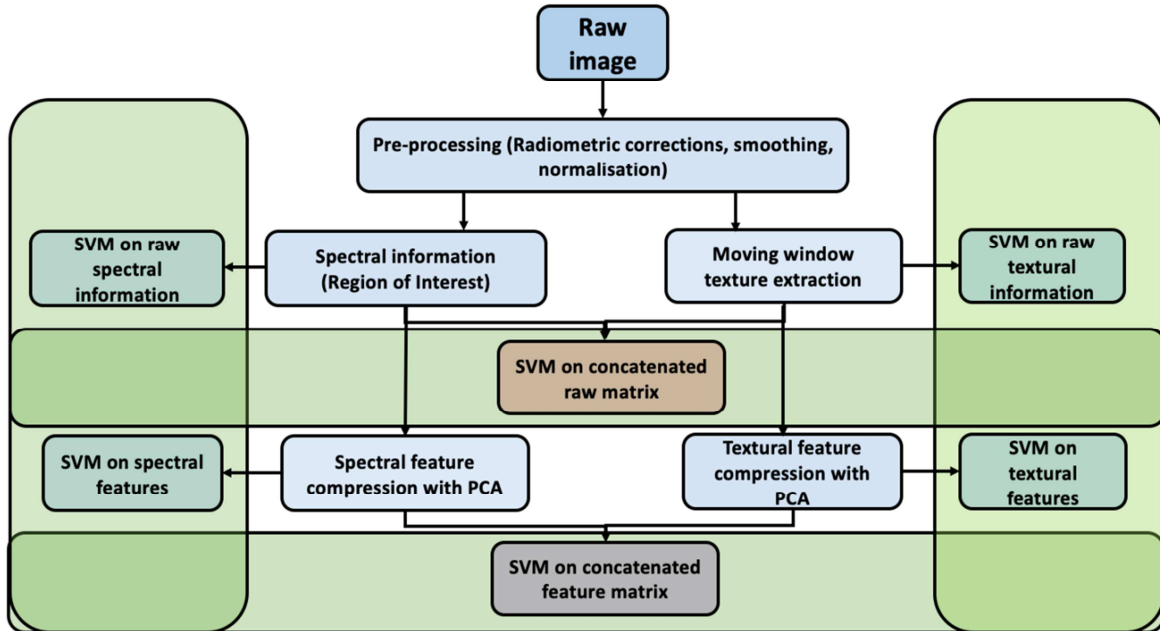


Figure 2: Schematic for raw data-level and feature-level fusion.

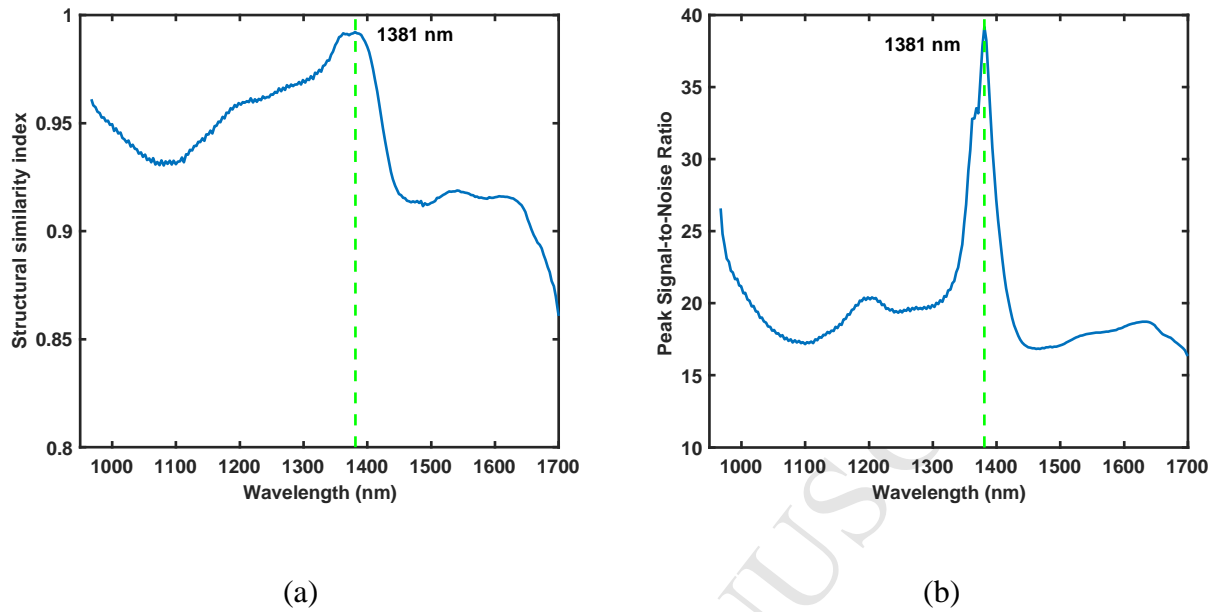


Figure 3 : Criteria used for selection of the best image plane on which to perform sharpening and textural analysis: a) SSIM and b) PSNR for all image planes in the range 967.11 – 1700 nm.

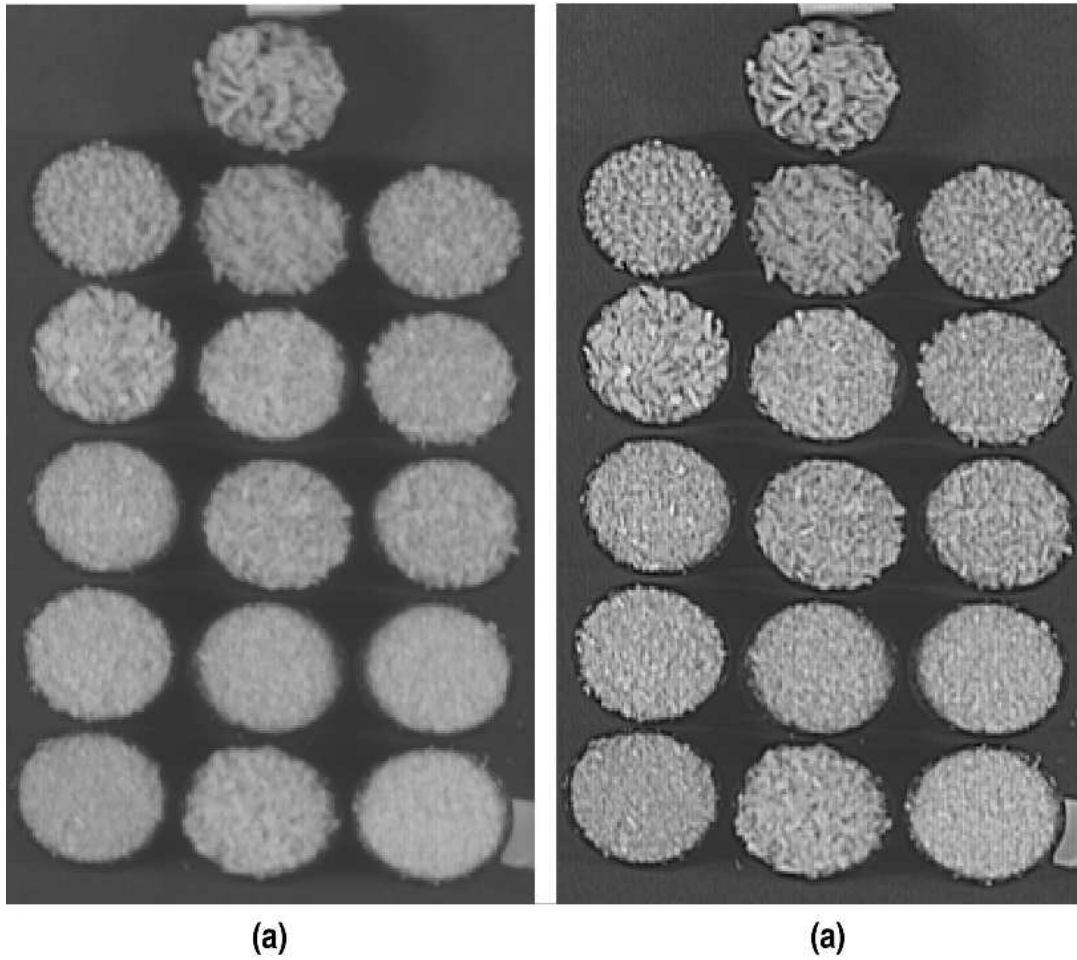


Figure 4 : Greyscale images produced using the image plane at 1381 nm (a) without and (b) with sharpening.

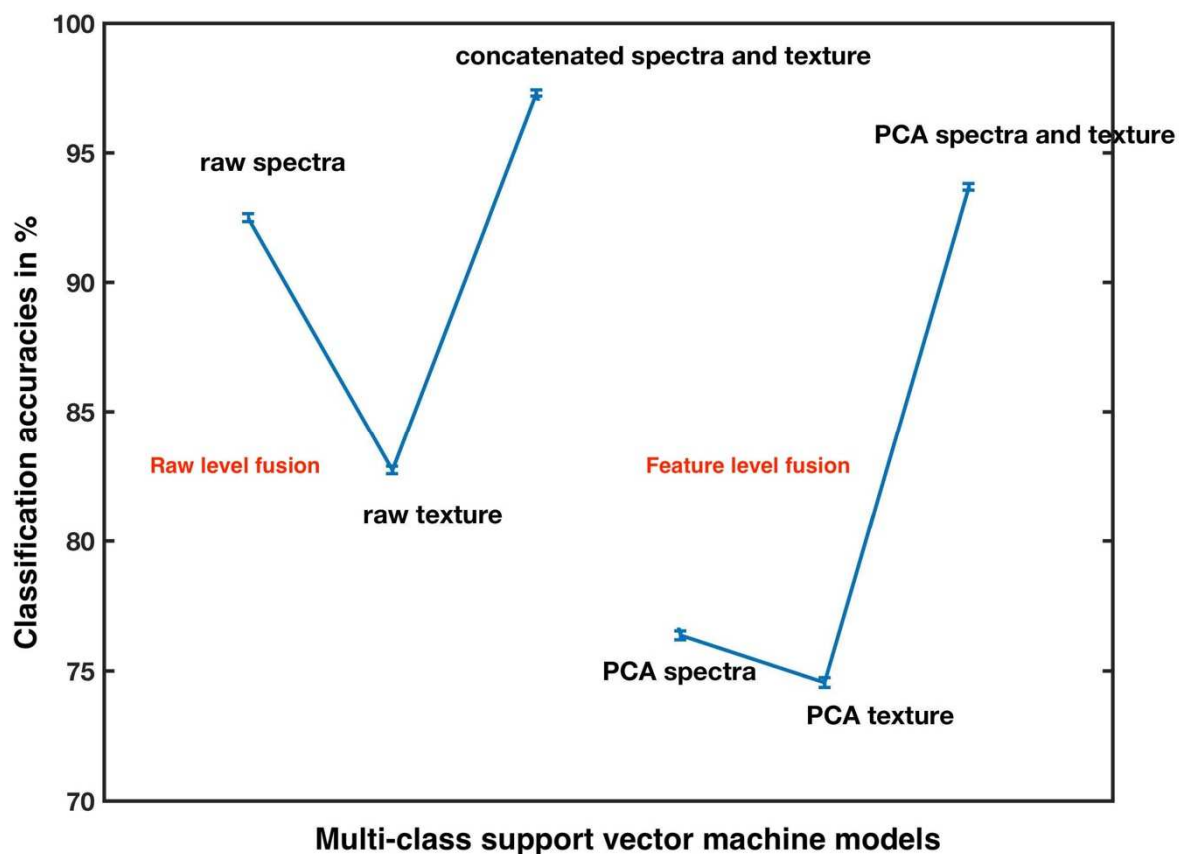


Figure 5 : Mean classification accuracies (in percent) of the 16 green tea products obtained for the calibration samples (pixels) using models built with raw data and PCA features. In both cases, models were built using spectral information alone, textural information alone and fused spectral and textural information. The error bars denote ± 1 standard deviation ($n = 100$).

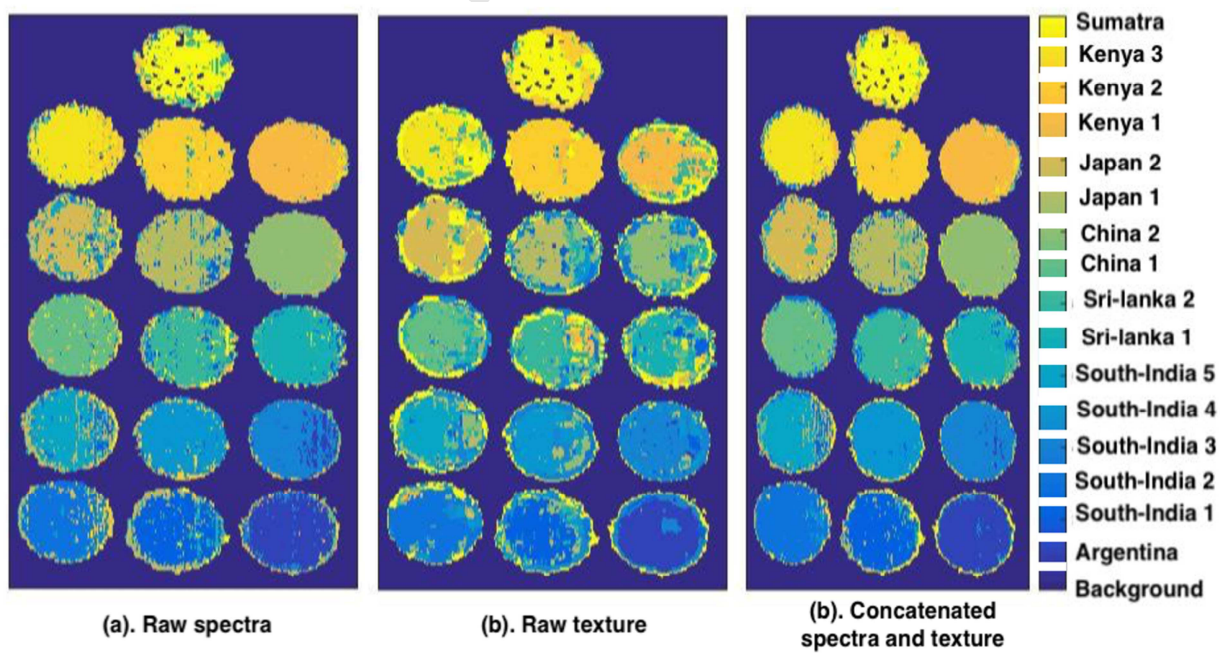


Figure 6 : Classification maps for the 16 green tea products obtained from SVM modelling of (a). raw spectral information, (b). raw textural information, and (c). concatenated raw spectral and textural information.

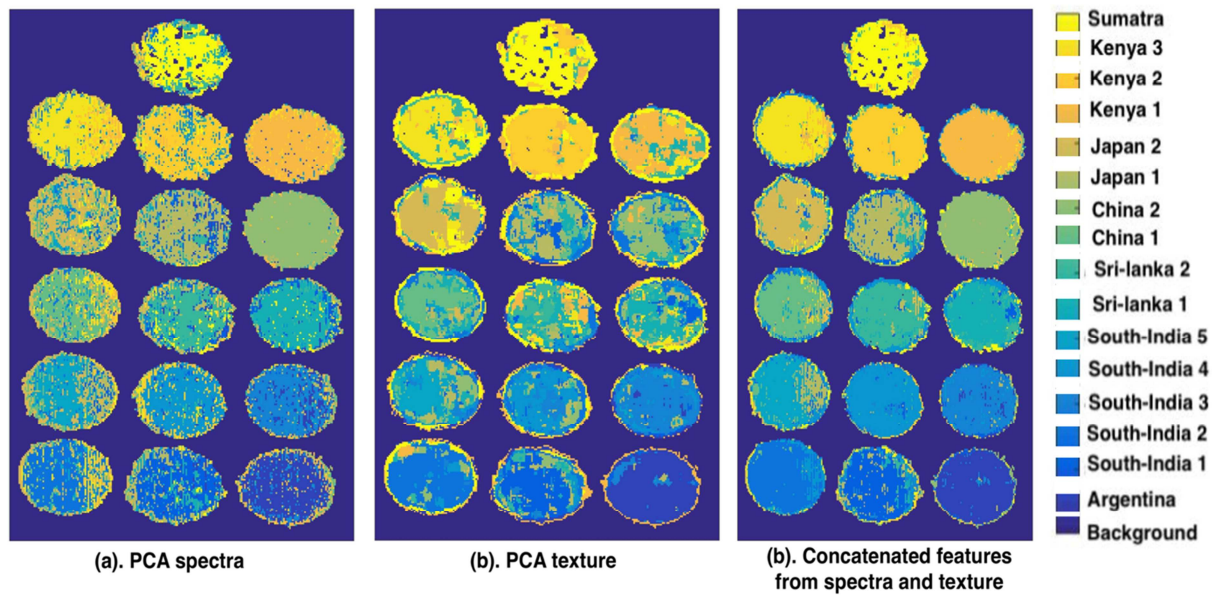


Figure 7 : Classification maps for the 16 green tea products obtained from SVM modelling of (a). PCA features extracted from spectral information, (b). PCA features extracted from textural information, and (c). concatenated PCA features from spectral and textural information.

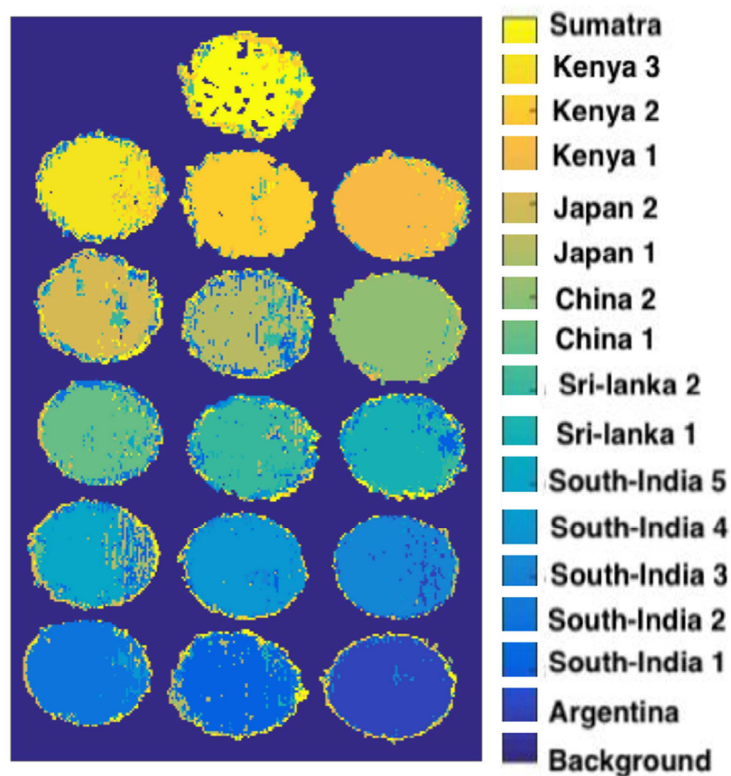


Figure 8 : Classification maps for the 16 green tea products obtained from decision-level data fusion, using a majority voting scheme, of the six classification maps obtained from SVM modelling of spectral information, textural information, and spectral and textural information using raw data (Figure 6) and PCA features (Figure 7).

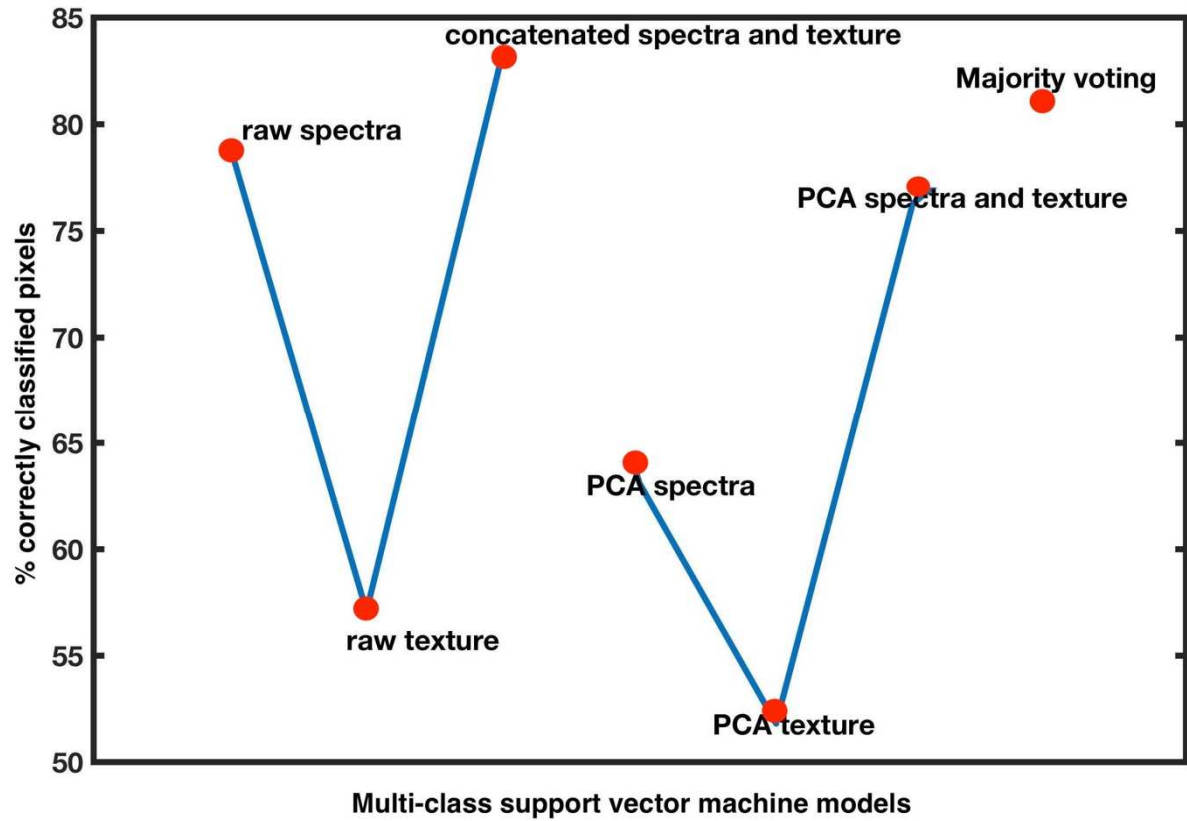


Figure 9 : Percentage of pixels correctly identified in the classification maps for the 16 green tea products obtained using six different SVM models and decision-level fusion by majority voting.

Research highlights

- Green tea products were analysed by near infrared hyperspectral imaging
- Textural information was extracted from the grey level co-occurrence matrix
- Textural properties were fused with near-infrared spectral information
- Data fusion improved the classification accuracy for green tea products